energies

MDPI

Review

Heat Transport in Rotating Annular Duct: A Short Review

Maxime Piton [1], Florian Huchet [1,*], Bogdan Cazacliu [1] and Olivier Le Corre [2]

[1] MAST-GPEM, University Gustave Eiffel, F-44344 Bouguenais, France
[2] IMT Atlantique Département Systèmes Énergétiques et Environnement, UMR CNRS GEPEA, F-44007 Nantes, France
* Correspondence: florian.huchet@univ-eiffel.fr

Abstract: Heat transport in rotating processes finds a wide range of application in which academic issues in the fluid mechanics and heat transfer areas are here reported. This paper discusses successive works from the seminal paper of Taylor (1923) to recent numerical results established from a broad range of methods such as DNS, LES, RANS or LB methods. The flow regimes identification is thus reported in Taylor–Couette geometry. The role of the axial flow rates in the apparition, stabilization and destruction of the large-scale of the turbulent structures is depicted in the case of Taylor–Couette–Poiseuille geometry. In a non-isothermal condition, a discussion is held on the various exponent values found in the scaling relationships relying on the Nusselt number as a function of the Rayleigh or Reynolds numbers according to the regimes of thermal convection.

Keywords: rotational energy process; vortex; instabilities; turbulence; thermal convection

Citation: Piton, M.; Huchet, F.; Cazacliu, B.; Le Corre, O. Heat Transport in Rotating Annular Duct: A Short Review. *Energies* **2022**, *15*, 8633. https://doi.org/10.3390/en15228633

Academic Editor: Lyes Bennamoun

Received: 30 September 2022
Accepted: 13 November 2022
Published: 17 November 2022

1. Introduction

Heat transport throughout rotating annular geometries covers a large spectrum of applications from natural to engineering domains. In the energy systems, it has shown great potential for the rotating wall cooling systems of electrical engines [1], turbine generators [2], rotary kilns [3], supercritical CO_2 extraction [4], and nuclear fusion reactors [5], to cite a few examples. The physical problems are shown in Figure 1 in the cylindrical coordinate system (r, θ, z).

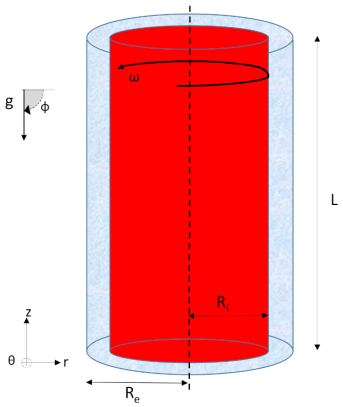

Figure 1. Position of the problem: two concentric cylindrical surfaces of inner and external radius, R_i and R_e, and of length, L, are inclined at an angle φ with the gravity. The rotation can be exerted from the inner (drawn here) or from the external cylinder at an angular velocity, ω. The heat gradient, $\partial T/\partial r$, can be imposed from any wall surface (the inner cylinder is chosen here), while the fluid motion is flowing into the gap, $e = Re - Ri$.

The inclination of the system with the gravity is aimed to work under vertical, horizontal or inclined orientations. The fluid motion is performed in the annular gap. The

heat flux density can be exerted from the external or the inner surface in order to impose a radial temperature difference. Under an isothermal condition, the influence of the curved wall upon the Dean vortices apparition is a first class of instabilities known in annular geometry. The rotational effect of the inner or external wall has resulted in a second class of instabilities. Such flows type are known under the name of Rotor–Stator cavities [6], Taylor–Couette [7] or Taylor–Couette–Poiseuille [8] if an axial flow rate is superimposed to the rotation. They have the particularity of reaching a high level of complexity from the point of view of the turbulence properties. Indeed, the turbulence is auto-sustained by the rotation effect that differs from a traditional wall-bounded flow, for which it is necessary to impose an external forcing to suppress the turbulence decay [9]. The centrifugal and axial motions are driven from a set of dimensionless numbers; the axial Reynolds number, Re_a, Taylor, Ta, or rotational Reynolds numbers, Re_w, themselves function of the torque number and geometric parameters [10]. As the Taylor number is increased, organized vortices appear and different flow regimes have been reported. The characterization of these secondary flows from their apparition and destabilization until their destruction at elevated Ta is still a topic of interest. The density-stratification induced by the momentum transport in such geometry is of practical interest for sediment transport in the ocean [11]. Such applications have also been explored for yield-stress fluid, where the flow regimes are different from the Newtonian case. The yield stress tends to stabilize the flow [12]. More recent work [13] supports such a conclusion, showing that two regions coexist, a shear-banding zone (flowing zone) and a dead zone (static zone) at an elevated shear rate.

Under a non-isothermal working condition, the axial flow rate is aimed to release the recovered heat waste, leading to various regimes of thermal convection [14]. The addition of grooves to the inner or outer wall raises the heat transfer magnitude [15]. The thermal stratification, in the sense of the mixed and natural convection, plays a major role in the performance of the annular heat exchanger. According to the geometrical characteristics of the annular passage [16] or the magnitude [17] and direction of the temperature gradient [18], the buoyancy forces will affect the flow regimes identified in the isothermal case. Numerous studies have also been conducted on nanofluids at low volume fraction concentration, Φ_v [19]. The thermal instabilities have an impact on the heat transfer for such Newtonian fluids [20]. For non-Newtonian fluid suspension, the rheological behavior of yield-stress fluid is recognized to be sensitive to the heat flux only at a weak imposed shear rate inferior to 0.02 s^{-1} [21], and that is why few experimental works have been explored in non-isothermal conditions except in forced convection [22]. Therefore, most of the following works were performed in more simple geometry to characterize convective heat transfer coefficients in circular ducts in a large range of axial flow rates [23,24].

Table 1 recaps the range of values reported in various applications of the literature.

Table 1. Rotating annular flow: range of applicability and literature examples.

Control Parameters	Lower Values	Upper Values
e **(m)**	$e = 0.01$ Microelectronics cooling device [25]	$e = \infty$ Space vehicle technology, ball bearing [26]
L**(m)**	$L \to 0$ Gas turbine discs cooling [27]	$L > 0$ Heat recovery of burners [28]
ω**(rpm)**	$\omega = 50$–114 Bioreactor for culture cells [29]	$\omega = 30,000$ CO_2 turbine diffuser [4]
Angle $\varphi(^\circ)$	$0 \leq \varphi < 90$ Double-pipe heat exchanger [19]	$\varphi = 90$ Vertical thermal energy storage tank [30]
$\partial T/\partial r$ $(^\circ$**C**$/$**m**$)$	-1 Geostrophic motion [31]	$+1$ Most of the applications [14,15]
Φ_v , $\Phi_w(-)$	$0.01 < \Phi_v < 0.1$ Al_2O_3/water Nanofluids [19]	$0.006 < \Phi_w < 0.2$ Viscoplastic type fluid [32]

While important reviews have been conducted on simple annular geometry without a rotating effect for a double-pipe heat exchanger application [19,33], there are, according to our knowledge, no reviews that focus on the heat transport in rotating annular ducts. The benefits of this review are to reach triple objectives covering the theory development, the applications and the modelling aspects.

2. Iso-Thermal Condition

In an isothermal case, the study of the vortex motion is a subject that has been widely studied for the last century in the scientific community. The interest of vortex flows lies in the possibility to significantly increase heat transfer while minimizing energy costs. Depending on the geometry adopted, the vortices produced may or may not be maintained throughout the flow. As an example, we briefly present the centrifugal instabilities that occur when using concave and/or convex walls (Figure 2):

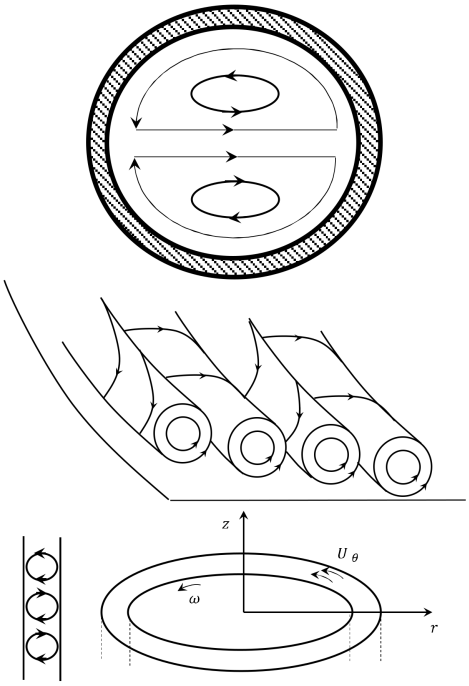

Figure 2. From bottom to top; Taylor vortices, Dean Vortices, and Görtler Vortices at a concave wall.

- The Taylor-Couette instability is a vortex confined between two coaxial cylinders with the outer cylinder stationary and the inner cylinder rotating at a constant angular velocity.
- The Dean instability is a flow induced by the curvature of the streamlines of a fully developed Newtonian flow. Above a critical value of the Dean number, a pair of vortex cells appears within the flow near the outer wall of the pipe.
- The Görtler instability is a secondary flow appearing in the boundary layer of the flow along a concave wall. This flow appears as longitudinal rolls, counter-rotating in pairs, aligned in the direction of the mean flow. Its appearance is caused by a competition between pressure and centrifugal forces.

2.1. Taylor-Couette Flow

Taylor–Couette flow occurs between two concentric cylinders of radius R_i for the inner cylinder and R_e for the outer cylinder in rotation (Figure 2). This flow has been extensively studied in the literature since Taylor's early work in 1923 [34], and remains a major topic of study in the fluid mechanics area.

The Taylor–Couette flow has a succession of very rich bifurcations generating more and more complex flows, finally leading to the turbulence. The different instabilities appear in the flow with the increase of the rotation velocity of the cylinder. When the angular

velocity of the cylinder exceeds a critical value ω_c, a first instability appears, forming a pair of counter-rotating toroidal vortices regularly spaced along the axis surrounding the cylinder like a vortex ring. These vortices are often referred to in the literature as the "Taylor roll" or "Taylor-Görtler instability" (Figure 3). This instability is generic, i.e., likely to occur in any flow deflected by a wall creating a pressure gradient normal to the streamlines.

Then, when a small axial flow is added to the Taylor–Couette flow, advection of the vortices occurs from the axial flow without being destroyed. Taylor (1923) [34] was the first to observe the instability of a fluid confined between two coaxial cylinders with a rotating inner cylinder. Subsequently, a series of theoretical, experimental and numerical works followed the seminal work of Taylor (1923) [34], Coles (1965) [35]; Fenstemacher (1979) [36]; and Andereck et al. (1986) [37]. Since the work of Taylor (1923) [34], many studies have been performed on the flow regimes identification in Taylor–Couette geometry. This is very complex and depends on operational and geometric parameters.

The Couette flow is laminar and stationary. It is driven by the viscous forces acting on the fluid and the annular streamlines centered on the rotation axis of the cylinder. Before the first instability, for low rotational speeds, Couette flow is simply characterized by the angular velocity $U_\theta(r)$. Solving the Navier–Stokes equations under suitable boundaries conditions leads to the following analytical solution:

$$U_\theta(r) = \omega \frac{1}{R_e^2 - R_i^2} \left[\frac{R_i^2 R_e^2}{r} - r R_i^2 \right] \quad (1)$$

Thus, in this study configuration, with only the inner cylinder in rotation, we systematically have the appearance of instabilities due to the increase of the rotation speed. The first instability is characterized by the appearance of stationary cells of toroidal shape, counter-rotating, associated in pairs and regularly ordered in the axial direction. Taylor determined the critical value of the inner cylinder velocity ω_c where the first instability is observed for a critical shape factor $\eta \to 1$. This rotational velocity ω_c leads to a critical value of the Taylor number $Ta_c = 1708$. Since Taylor's early work, several empirical or analytical correlations have been presented to evaluate this threshold. The most widely used correlation was defined by Esser and Grossmann (1996) [38]:

$$Re_{\omega_c} = \frac{1}{\alpha^2} \frac{(1+\eta)^2}{2\eta\sqrt{(1-\eta)(3+\eta)}} \text{ avec } \alpha = 0.1556 \quad (2)$$

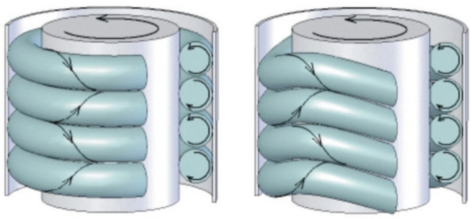

Figure 3. Taylor cells (**Left-hand**) and Wavy Taylor cell (**Right-hand**) [39].

In the case where the rotational speed increases and the Taylor number exceeds the second threshold, $Ta_{c,2}$, the presence of a new instability was demonstrated by Coles (1965) [35]. He observed the presence of ripples at the dividing lines of the Taylor cells. The Taylor cells are no longer perpendicular to the axis of the cylinder, but rather show a wavy behavior. The axisymmetric flow becomes unstable and unsteady and therefore doubly periodic, characterized by an axial and azimuthal wavenumber. When the Taylor number exceeds a third threshold, $Ta_{c,3}$, the flow becomes more complex. The amplitude of the ripples varies periodically, and the flow has two temporal frequencies. With the increase of the Taylor number, the flow behaves as wavy, and weakly turbulent before the flow becomes fully turbulent, suppressing the azimuthal wave.

The transitions observed in the flow do not only depend on the Taylor number, but also on the previous history of the flow, implying a hysteresis phenomenon depending on the way in which the rotational speed studied is reached. This dependence on the history of the flow was observed by Cole (1965) [35] on experiments, which revealed 26 different states for the same Taylor number.

The Taylor–Couette flow is a complex problem despite the fact that it has been the subject of many studies and that many questions remain unanswered today. The structure of the flow depends on several geometrical or operational parameters such as η, the shape factor, Γ, the aspect ratio and the Taylor number, Ta, as well as the non-uniqueness of the flow.

2.2. Taylor–Couette–Poiseuille Flow

Superimposing an axial flow on the Taylor–Couette flow increases the complexity of the flow. The Taylor–Couette–Poiseuille flow has a new dynamic parameter added to the inner cylinder rotation speed ω: the mean axial fluid velocity $\overline{U}_z$.

The flow structure results from the superposition of two mechanisms, the first related to the effects of rotation and the second to the axial flow. From these mechanisms, two main transitions can be distinguished: the transition from laminar to turbulent flow with increasing axial velocity, and the transition from turbulent flow to the appearance of vortex structures above the critical rotational speed ω of the cylinder. The combination of these combined phenomena was described by Kaye and Elgar (1958) [40] (Figure 4), who decompose into four mains flow regimes:

- Laminar flow,
- Laminar flow with Taylor structures,
- Turbulent flow,
- Turbulent flow with Taylor structures.

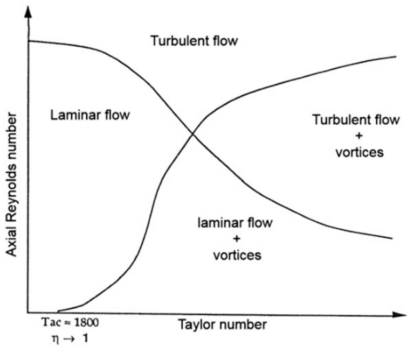

Figure 4. Flow regimes as a function of axial Reynolds number and Taylor number [41].

Kaye and Eglar (1958) [40] cited by [41] showed with an experimental study and a hot wire anemometer that axial flow has a stabilizing effect on Taylor structures. The onset of the first instabilities occurs for larger cylinder rotation speeds ω (higher Taylor number) than a simple Taylor–Couette flow. The importance of rotational velocity in flow transitions is important and is the subject of many studies.

The flow characterization has been established by various works inventoried on the subject [42–44] for $0 \leq Re_a \leq 10^4$ and $0 \leq Ta \leq 10^6$. A study with larger axial and Taylor Reynolds numbers was also performed [45] ($2 \times 10^4 \leq Re_a \leq 3 \times 10^4$, $4 \times 10^7 \leq Ta \leq 2 \times 10^9$). The authors investigated the influence of physical phenomena such as the rotation speed of the inner cylinder on the transfer phenomena as a function of the identified flow regime. Experimental results [43] show that the transition between a turbulent flow and a turbulent flow containing Taylor cells is punctuated by a transition zone and not distinctly separated. Jakoby et al. (1999) [45] also confirmed the existence of a transition zone between a flow with and without Taylor cells.

A more detailed analysis of the transitions was performed experimentally [46] cited by [41]. This experimental study was performed for low Taylor numbers ($Ta < 3000$) and very low Reynolds numbers ($Re_a < 540$) in the context of a weak annular gap $\eta = 0.885$ and $\Gamma = 41$. They observed a significant number of flow regimes ranging from laminar to turbulent flow. The limited description at low Reynolds and Taylor numbers is presented by a detailed flow mapping (Figure 5).

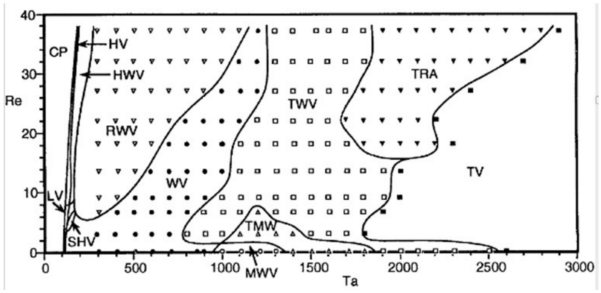

CP	Couette–Poiseuille flow
HV	Laminar helical vortices
HWV	Laminar helical wavy vortices
LV	Laminar vortices
MWV	Laminar modulated wavy vortices
RWV	Random laminar wavy vortices
SHV	Stationary helical vortices
TMW	Turbulent modulated wavy vortices
TRA	Transitional flow
TV	Turbulent vortices
TWV	Turbulent wavy vortices
WV	Laminar wavy vortices

Figure 5. Different transitions of the Taylor–Couette–Poiseuille flow [41].

Finally, several authors have focused on the parameters influencing the transition between flow with and without Taylor cells. The size of the annulus (Γ, η) appears to play an important role in the flow transitions (Figure 6). Kaye and Eglar (1958) [40] cited by [41] determined and compared the major flow transitions for two annular space thicknesses $\eta = 0.693$ and 0.802. For very low axial flow or Reynolds number ($Re_a < 100$), the size of the annular space does not appear to influence the transitions. In contrast, for high axial Reynolds number, increasing the annulus size seems to alter the flow transition. Taylor cells appear for lower angular velocity of the inner cylinder. Similar results have also been observed [45] on the transition between a flow with and without Taylor cells.

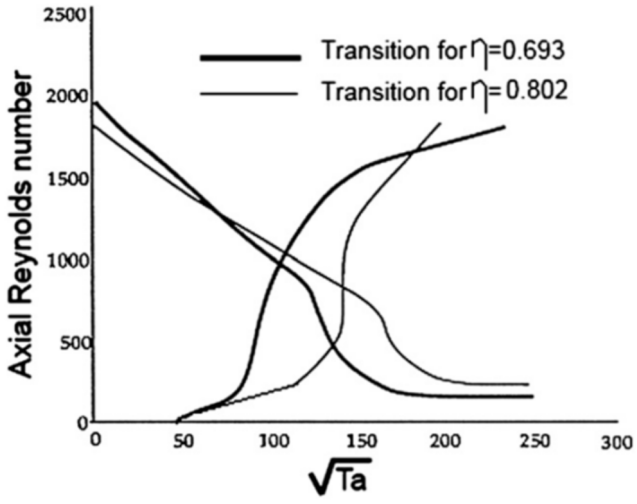

Figure 6. Taylor and axial Reynolds number flow transition: Influence of annulus thickness [41].

In contrast to the results of Kaye and Eglar (1958) [40], other work [47] showed that widening the annulus stabilized the flow, with an appearance of Taylor cells for larger Taylor numbers. This contradiction between the authors can be explained by the effect of L and Γ on the development of the flow and specifically the axial velocity profile. Increasing Re_a has the effect of increasing the flow developing region, and thus delaying along the z-axis the appearance of the first Taylor cells [48].

Fénot et al. (2011) [49] performed a literature review on heat transfer in Taylor–Couette, and Taylor–Couette–Poiseuille flows. They concluded that:

"Despite the considerable amount of studies carried out on Taylor-Couette-Poiseuille flow, the large number of influential factors leaves many questions regarding their impacts

on flow dynamics and heat transfers". Indeed, the results published in the literature depend largely on the study configuration, and do not yet provide a sufficient basis for large-scale extrapolation.

2.3. Numerical Simulation in Taylor–Couette–Poiseuille Flow

Numerical studies of Taylor–Couette–Poiseuille flow cover different configurations of the flow and have already received much attention due to the three-dimensional boundary layer of the flow. Some of the different numerical studies of the Taylor–Couette–Poiseuille flow available in the literature are presented in Table 2. The experimental studies [50,51] provide valuable experimental data on the influence of the rotating inner wall on the axial flow in an annular space. These authors [50,51] extracted the various components of mean velocity and turbulent stresses in an annular space possessing a large shape factor ($\eta = 0.5$) and a large aspect ratio ($\Gamma = 98$–244; $N \to \infty$). These experiments included the study of the effect of the nature of the Newtonian and shear-thinning fluid on the flow. Finally, the large aspect ratio, Γ, used by the authors during their experiments allows for the assumption of fully developed flow in the axial direction. These experimental data [50,51] were used to validate most of the numerical experiments in Taylor–Couette–Poiseuille flow recapped in Table 2.

Authors [52,53] numerically investigated, from DNS [52] and LES [53], the effect of the radius of curvature of two annular geometries ($\eta = 0.1$ et 0.5) upon the near wall turbulent structures in a given axial flow ($Re_a = 4450$). In this study, the outer and inner cylinders are stationary. The authors showed a change in the characteristic of the turbulent structures at the outer wall due to the change in the radius of curvature. Later, Jung and Sung (2006) [54] extended the numerical study [52] with a rotating inner wall. The rotation parameter $N = Re_t / Re_a$ studied by the authors was 0.429. They were interested in the study of coherent structures located in the inner wall and their changes compared to the study of Chung et al. (2002) [52] due to the influence of centrifugal forces. The authors found an increase in near-wall turbulence with an increase in the ejection of coherent structures into the flow.

Chung and Sung (2005) [53] performed a numerical study by Large Eddy Simulation (LES). The LES simulation was performed using the experimental setup from [50] ($\eta = 0.5$ and $= 0.214,\ 0.429$ and 0.858 for an axial Reynolds number $Re_a = 4450$). They showed the influence of the inner cylinder rotation velocity on the destabilization of the turbulent structures in the near wall region.

Large-Eddy Simulation was also used [55] to characterize a Taylor–Couette–Poiseuille flow with a shape factor $\eta = 0.5$. The study regards a rotating outer cylinder, which is rarer in the literature. This study focuses on the effect of rotation for a wide range of studies of the rotation parameter N, ranging from 0.5 to 4. The authors focused on studying the effect of the outer cylinder velocity on the mean flow, turbulence statistics and vortex structures (Q-Criterion). A significant change in the turbulent structures was observed for $N = 2.8$. Indeed, the turbulence is thus reduced while helical vortex structures are perceptible in the near outer wall. According to the authors [55], this change is attributed to the centrifugal turbulence generated in the near wall dominating the inertial forces of the flow. For a higher rotation rate ($N = 4$), the flow stabilizes and becomes laminar with the appearance of Taylor–Couette vortex structures usually observed in a Taylor–Couette flow without axial flow.

Table 2. Numerical and experimental studies in TC and TCP flows identified in the literature.

Authors	Method	η	Γ	Flow Regime	Re_a	Re_ω,Ta	N
Nourri and Whitelaw (1994) [50]	LDA	0.5	98	Turbulent	8900	$Re_\omega = 3818$	0.429
Escudier and Gouldson (1995) [51]	LDA	0.506	244	Turbulent	2400; 5000; 15,000	$Re_\omega = 1922$	0.80; 0.38; 0.13
Chung et al. (2002) [52]	DNS	0.1–0.5	-	Turbulent	8900	$Re_\omega = 0$	-
Chung and Sung (2005) [53]	LES	0.5	-	Turbulent	8900	$Re_\omega = 1909; 3818; 7636$	0.214, 0.429; 0.858
Jung and Sung (2006) [54]	DNS	0.5	-	Turbulent	8900	$Re_\omega = 3818$	0.429
Hadziabdic et al. (2013) [55]	LES	0.5	-	Turbulent	12,500	$6250 \leq Re_\omega \leq 50,000$	$0.5 \leq N \leq 4$
Poncet et al. (2014) [56]	LES	0.889	10	Turbulent	$7490 \leq Re_a \leq 11,234$	$16,756 \leq Re_\omega \leq 50,266$	$1.49 \leq N \leq 6.71$
Poncet et al. (2011) [57]	RANS (RSM)	0.961	76.9	Laminar-Turbulent	$0 \leq Re_a \leq 41,254$	$7488 \leq Re_\omega \leq 74,886$	$0.18 \leq N \leq +\infty$
Pawar and Thorat (2012) [58]	RANS (RSM)	0.745	5.85–1	Turbulent	0	$1 \leq Ta \leq 11,684$	
Nasser et al. (1990) [59]	RANS $(k-\varepsilon)$	0.5	244	Laminar-Turbulent	7400	$Re_\omega = 1904$	0.13
Ohsawa et al. (2016) [60]	LES	0.87	18	Turbulent	$500 \leq Re_a \leq 8000$	$Ta = 4000$	$1 \leq N \leq 16$
Mehrez et al. (2019) [61]	Lattice Boltzman	0.5–0.6–0.7	2–3.8–5–6–7–8–9–10	Laminar-Wavy	$0 \leq Re_a \leq 17$	$30 \leq Ta \leq 270$	
Piton et al. (2022) [62]	LES & RANS (RSM)	0.809	10	Turbulent	$1462 \leq Re_a \leq 8776$	$Re_\omega = 7488$	$1.71 \leq N \leq 5.12$

Poncet et al. (2014) [56] performed Large-Eddy Simulations of a Taylor–Couette–Poiseuille flow with rotation of the inner cylinder in a narrow annular space, but for large values of the rotational parameter N ($1.49 \leq N \leq 6.71$). Initially, the authors compared their numerical results favorably on the experimental data [50], and on the data from Large Eddy Simulations [53]. Next, the authors extended their work to real operating conditions ($\eta = 0.889$, $\Gamma = 10$) to study the influence of the rotation parameter N on the mean flow and on the turbulence statistics. The authors were also interested in the nature of the coherent structures appearing in the boundary layer and their influences on the heat transfers. The authors Poncet et al. (2014) [56] observed that the turbulence is mainly concentrated in the boundary layer of the flow. A small dissymmetry is noticeable in the Reynolds stress distribution at the rotating cylinder boundary layer, telling us that the inner cylinder boundary layer is more chaotic than that observed on the outer cylinder. Rotation of the inner cylinder appears to destabilize the flow and have an opposite effect compared to the results obtained by Hadziabdic et al. (2013) [55] of stabilizing the flow with increasing rotation of the outer cylinder.

In the literature, there are a few numerical simulations of Taylor–Couette–Poiseuille flow using the Reynolds decomposition known as RANS (Reynolds Averaged Navier–Stokes). The $k - \varepsilon$ turbulence model is the most commonly used model in computational fluid mechanics to simulate the mean flow under turbulent conditions. Nevertheless, the predictions from a $k-\varepsilon$ turbulence model seem to deviate to the literature results in the case of a Taylor–Couette–Poiseuille flow. Indeed, in a flow where turbulent transport and no equilibrium effects are important, the assumption of turbulent viscosity used by the $k - \varepsilon$ model is no longer valid, and the results of the turbulent viscosity model may turn out to be not accurate [57,58]. Some authors [59] have used a $k - \varepsilon$ turbulence model, but it shows large discrepancies compared to the experimental data of [51]. Compared to turbulent viscosity models, Reynolds stress models (RSM) naturally include curvature effects, abrupt changes in velocity stress, and secondary flows. The Reynolds stress model solves the transport equations for each Reynolds stress ${u'}_i{u'}_j$ and dissipation rate ε at each time step. The authors of [57] performed steady state RANS simulations based on an innovative Reynolds stress model sensitized to rotational effects. A study [57] has compared their results favorably on the experimental data of Escudier and Gouldson (1995) [51], and extended their work on real operating conditions ($\eta = 0.961$, $\Gamma = 77$) including non-isothermal flow in a wide range of Reynolds numbers ($0 \leq Re_a \leq 4870$, $3744 \leq Re_w \leq 37,443$). Recent work addresses numerical simulations from various methods to understand the role of the wall turbulence properties in the heat transfer results in non-isothermal conditions. Ohasawa et al. (2016) [60] used LES simulation, showing a large contribution of the turbulent transport term on the Nusselt number results. Mehrez et al. (2019) [61] used the Lattice Boltzmann method to assess the importance given to the initial conditions for Taylor–Couette–Poiseuille flow characterization. Piton et al. 2022 [62] used LES method to characterize the turbulent kinetic energy transport in the near wall region for heat recovery system application (Figure 7). Therefore, the importance to study the rotational annular duct in a non-isothermal condition has a practical interest (see Table 1). The next section is aimed to cover the main fundamental works that have included the heat transfer phenomenon.

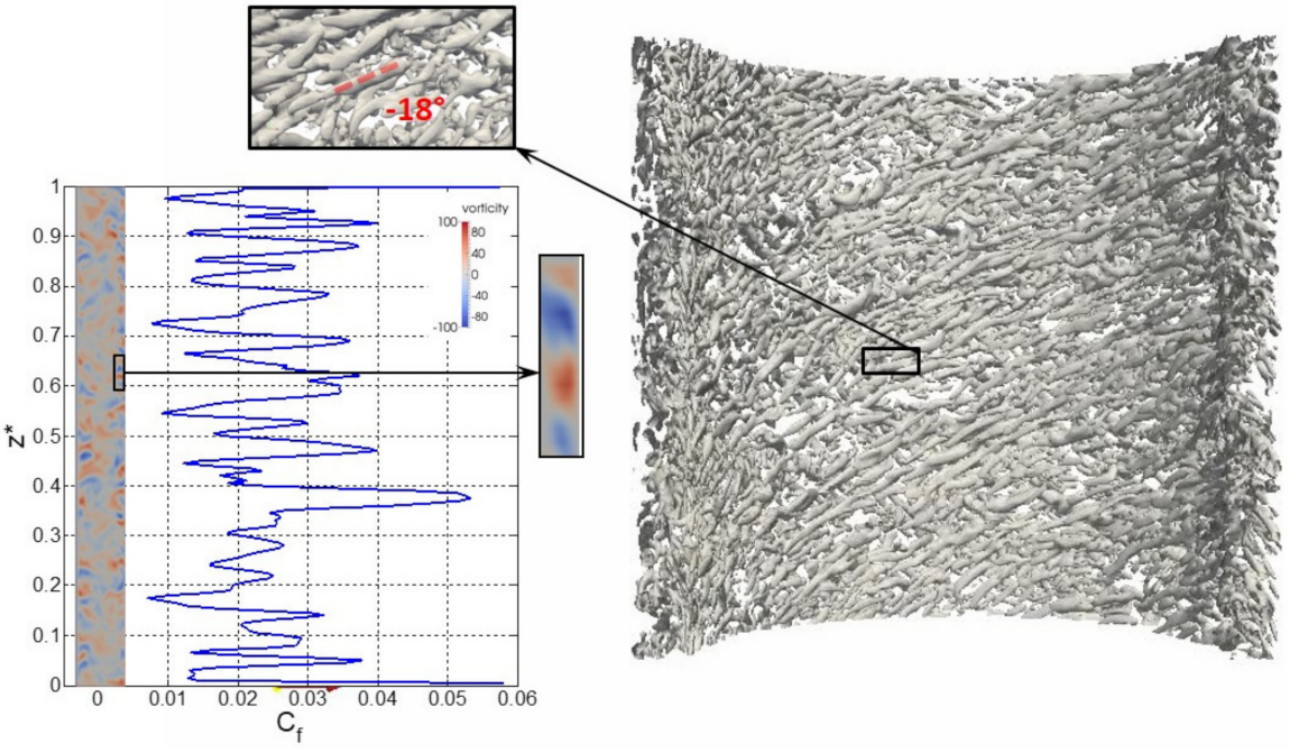

Figure 7. Simulation LES in the near-wall region of a Taylor–Couette–Poseuille flow. Q-criterion applied for angular assessment of the vortex [41].

3. Non-Isothermal Condition

We can report a large amount of convection studies that investigated annular ducts for which constant temperature or constant heat fluxes is imposed at the inner or outer boundaries. According to a careful sorting extracted from the literature, the present section addresses a report of the main scaling laws of the heat transport in rotating annular ducts.

In natural and mixed regimes of convection, the buoyancy force driven by the difference of fluid density in the annulus cannot be neglected. The momentum and buoyancy induced flows increase the complexity of the hydrodynamics behavior. It implies a large variety of flow patterns, from spiral-type at low rotational speed to Taylor Vortex-type at the dominant torque effect [63]. The Rayleigh number, Ra, is the dimensionless number allowing us to express the importance of the buoyancy force driven by the difference of temperature. It is defined according to the following relationship:

$$Ra = \frac{g\beta(T_{REF} - T_{Wall})(D)^3}{\nu\kappa} \tag{3}$$

where T_{wall} is the hot temperature source at the inner or outer wall, T_{REF} can be varied according to the author. Generally, it corresponds to the fluid temperature probed in the vicinity of the inner or outer wall. g is the gravity, D the external cylinder diameter, β, ν and κ are, respectively, the dilatation coefficient, the kinematic viscosity and the thermal diffusivity of the fluid.

At a low Ra number below Ra_c = 400 Γ, the buoyancy-induced flow are weak [16], a purely diffusive regime is considered. The Nusselt number, which characterizes heat transfer, is solely dependent on the geometry of the annular cell [64] and defined by:

$$Nu = \frac{qD_h}{(T_{REF} - T_{Wall})\lambda} = \frac{2\left(\frac{R_e - R_i}{R_i}\right)}{\ln\left[1 + \left(\frac{R_e - R_i}{R_i}\right)\right]} \tag{4}$$

With q the heat flux density, $D_h = 2e$ is the hydraulic diameter and λ the thermal conductivity.

From $Ra > Ra_c$ and $Ta < Ta_c$ the onset of convection in a closed-gap system is governed by the buoyancy force revealing scaling law of type $Nu{\sim}Ra^{\alpha\sim1/3}$ [16] in such way that:

$$Nu = 0.22Ra^{0.29} \quad (5)$$

The mechanism of transport would support the theory of Rayleigh–Bernard convection where the two thermal boundaries (inner and outer cylinders) are the engine of the fluid motion. In open-gap, the end-effects are not negligible, developing flow and additional turbulent transfer of momentum energy. The momentum kinetic energy coupled to the buoyancy forces from the thermal kinetic energy have shown that the scaling law is of the type $Nu{\sim}Ra^{0.38<\alpha<0.5}$ [65,66]. The scaling exponent, α, is variable in the literature [66]. Recent works seem shown that it depends essentially on the origin of the turbulent transport mechanisms, which are summarized by Swirling-type [14] and Rayleigh-type flow behaviors [67]. Thus, in the more recent works, effective Reynolds numbers are preferred to the Rayleigh number by adjusting the scaling exponent in such a way that $Nu \sim Re_{eff}^{\gamma}$ with Re_{eff} depending on Ra [68]. Recent results conclude to an exponent value close to γ~0.6 in axial [68] or radial heat fluxes conditions [14] such as:

$$Nu = 0.3{Re_{eff}}^{0.6} \quad (6)$$

DNS modelling and further experiments appear as a safe bet to overcome the physical complexity linked to multiple turbulent flow states and the coupling phenomena of heat and momentum transfer [63,68]. A set of correlations are depicted in Table 3.

Table 3. Scaling relationships obtained in rotating annular ducts in diffusive, natural and mixed regimes of convection.

Geometry	Authors	Range of Applicability	Nu-Correlation	Remarks
Closed gap	Bjorklund and kays (1959) [64]	Diffusive regime ($Ra < 400.\Gamma$) $Ta << Ta_c$	Equation (4)	Conduction
	Vahl Davis G. and Thomas (1969) [16]	$Ra > Ra_c$; $Ta << Ta_c$	Equation (5)	Natural convection
Open gap	Huchet et al. (2017) [14]	$2.5 \times 10^7 > Ra > 2.5 \times 10^8$ $0 < Re_w < 6980$ $1000 < Re_a < 15{,}000$	Equation (6)	Heated rotor–Mixed Convection

In forced regime of convection at large $Ta > Ta_c$, two reviewing papers were recapped most of the papers published before 2010. Howey et al. (2012) [69] were interested in air gap convection in rotating electrical machines, giving some results based on popular Nu-correlation showing that large gap ratios and higher rotational speed give better performance than smaller rotating machines. Fenot et al. (2011) [49] made a recapitulation of the main correlations for convective heat transfer in closed and open cylindrical gaps. The conjugated inertial effects of the axial and rotational flows lead to a complex behavior and scattered equation in terms of $Nu = f(Re_a, Re_w)$. Numerical works performed in the last decade have allowed understanding the role of the vortices transport (see Figure 7) on the heat transfer mechanisms [56,62]. It has resulted in a new set of correlations in terms of skin-friction factor and heat transfer in case of optimized geometries of TCP [70]. A set of correlations are depicted in Table 4.

Table 4. Scaling relationships obtained in rotating annular ducts in forced regime of convection.

Geometry	Authors	Range of Applicability	Nu-Correlation	Remarks
Closed-gap	Beker and Kays (1962) [71]	$1994 < Ta < 10^4$ $10^4 < Ta < 3.310^5$	$Nu_w = 0.128(Ta)^{0.367}$ $Nu_w = 0.409(Ta)^{0.241}$	Radial heat flux
Open gap	Gazley (1958) [72]	$Re_a < 12{,}000$ $Re_w < 110{,}000$	$\overline{Nu} = 0.03Re_{eff}^{0.8}$	Calculation made from T_{rot}-T_{st}
	Bouafia (1998) [1]	$11{,}000 < Re_a < 31{,}000$ $500 < Re_w < 31{,}000$	$Nu_w = 0.021Re_{eff}^{0.8}$	Heated rotor

4. Conclusions

To conclude, the objective of this review was to establish an overview of the theory development, the applications and the modelling aspects of the heat transport into rotating annular ducts.

The governing parameters of control were found to be widespread according to energy systems. Gap thickness, length of cylinders and rotational velocity can vary in an extreme way if gases, liquid or even non-Newtonian fluid are considered. From such a variety of configurations, it has resulted in numerous works in the literature to cover the entire flow regimes in Taylor–Couette (TC) geometry. The prediction of the instabilities according to the magnitude of the rotational velocity, shape factor and gap thickness remains a technological and scientific issue. The Taylor–Couette–Poiseuille (TCP) configuration has opened the way to expand laminar and turbulent flow regimes in order to better control the flow instabilities apparition with an imposed axial flow rate. Nevertheless, such a configuration reaches no less than 12 flow regimes according to the imposed rotational velocity and axial flow rates. Thus, many numerical results of the literature have been presented using various methods for turbulence characterization in TCP flow. It has been shown that LES seems a good candidate to model the flow dynamics in such geometries. LES is well adapted to characterize the near-wall region, where the transport of the turbulent kinetic energy is responsible for the heat transfer optimization, or defect, according to the importance of the axial flow rates.

In non-isothermal conditions, several works have been established for which the present review proposes to distinguish:

- The open- and closed-gap;
- The radial and axial heat flux densities.

Depending on the configuration, many correlations of the Nu number could be listed. In the natural regime of convection, the dependence in $Ra^{0.3}$ seems to be valid. In the mixed and forced regime of convection, respectively, it seems that the dependence in $Re_{eff}^{\gamma\sim0.6}$ and $Re_{eff}^{\gamma\sim0.8}$ finds consensus.

The future research direction will aim at an explanation of these exponents' values for heat transport scaling relationships. Only a conjugated effort of experience and modelling will be able to determine the origin of the turbulent flow mechanisms (i.e., buoyancy and/or inertia) responsible for the heat transport in the near wall region.

Author Contributions: Conceptualization, M.P. and F.H.; methodology, F.H.; software, M.P.; validation, M.P., F.H. and O.L.C.; formal analysis, M.P.; investigation, M.P.; resources, B.C.; data curation, F.H.; writing—original draft preparation, M.P.; writing—review and editing, F.H.; visualization, M.P.; supervision, F.H. and O.L.C.; project administration, F.H.; funding acquisition, B.C. All authors have read and agreed to the published version of the manuscript.

Funding: This research received no external funding.

Data Availability Statement: Not applicable.

Conflicts of Interest: The authors declare no conflict of interest.

Nomenclature

Symbols		
D	m	External diameter of the cylinder
D_h	m	Hydraulic diameter
e	m	Thickness of the annular space (=R_{e}- R_i)
g	m.s^{-2}	Gravity
k	m^2.s^{-2}	Turbulent kinetic energy
L	m	Length of the cylinders
N	-	Rotational parameters (=Re_t/Re_a)
Nu	-	Nusselt number
q	W/m^2	Wall heat density
R_i	m	Internal raduis
R_e	m	External raduis
Ra	-	Rayleigh Number
Re_a	-	Axial Reynolds number
Re_{eff}	-	Effective Reynolds number
Re_w	-	Rotational Reynolds number
T	°K	Temperature
T_{Wall}	°K	Wall temperature
Ta	-	Taylor number
Ta_c	-	Critical Taylor number
U_θ	m.s^{-1}	Tangential or spanwise velocity component
U_z	m.s^{-1}	Axial or streamswise velocity component
${u'}_i{u'}_j$	m^2.s^{-2}	Reynolds stress tensor
r, θ, z	(m, rad, m)	Cylindrical coordinate
r^*	-	Dimensionless radial coordinate $(= r - R_i)/(R_e - R_i)$
z^*	-	Dimensionless axial coordinate (=z/L)
Greek symbols		
β	°K^{-1}	Thermal dilatation coefficient
ε	m^3.s^{-2}	Turbulent kinetic energy dissipation rate
η	-	Shape factor ($= R_i/R_e$)
κ	m.s^{-2}	Thermal diffusivity
λ	W.m^{-1}.K^{-1}	Themal conductivity
Γ	-	Aspect ratio ($= L/e$)
ν	m.s^{-2}	Kinematic viscosity
φ	rad	
Φ_v	-	Volume fraction
Φ_w	-	Mass fraction
ω	rad.s^{-1}	Angular velocity of the cylinder
ω_c	rad.s^{-1}	Crictical angular velocity
Abbreviations		
DNS		Direct Numerical Simulation
LB		Lattice Boltzman method
LDA		Laser Doppler Anemometry
LES		Large Eddy Simulation
RANS		Reynolds Averaged Navier Stokes
TC		Taylor-Couette
TCP		Taylor-Couette-Poiseuille
$k-\varepsilon$		Turbulent closure model

References

1. Bouafia, M.; Bertin, Y.; Saulnier, J.-B.; Ropert, P. Analyse expérimentale des transferts de chaleur en espace annulaire étroit et rainuré avec cylindre intérieur tournant. *Int. J. Heat Mass Transf.* **1998**, *41*, 1279–1291. [CrossRef]
2. Yoo, W.; Jeon, S.; Son, C.; Yang, J.; Ahn, D.; Kim, S.; Hwang, K.; Ha, S. Full surface heat transfer characteristics of rotor ventilation duct of a turbine generator. *Appl. Therm. Eng.* **2016**, *94*, 385–394. [CrossRef]
3. Caputo, A.C.; Pelegagge, P.M.; Salini, P. Performance modeling of radiant heat recovery exchangers for rotary kilns. *Appl. Therm. Eng.* **2011**, *31*, 2578–2589. [CrossRef]

4. Swann, P.B.; Russel, H.; Jahn, I.H. Taylor-Couette-Poiseuille flow heat transfer in a high Taylor number test rig. *J. Glob. Power Propuls. Soc.* **2021**, *5*, 126–147. [CrossRef]
5. Lorusso, P.; Martelli, E.; Del Nevo ADel Narcisi, V.; Giannetti, F.; Tarantino, M. Development of a PbLi heat exchanger for EU DEMO fusion reactor: Experimental test and system code assessment. *Fusion Eng. Des.* **2021**, *169*, 112462. [CrossRef]
6. Poncet, S.; Schiestel, R. Numerical modeling of heat transfer and fluid flow in rotor–stator cavities with throughflow. *Int. J. Heat Mass Transf.* **2007**, *50*, 1528–1544. [CrossRef]
7. Nemri, M.; Charton, S.; Climent, E. Mixing and axial dispersion in Taylor-Couette flows: The effect of the flow regime. *Chem. Eng. Sci.* **2015**, *139*, 109–124. [CrossRef]
8. Abou-Ziyan, H.; Ameen, R.; Elsayed, K. Fluid flow and convection heat transfer in concentric and eccentric cylindrical annuli of different radii ratios for Taylor-Couette-Poiseuille flow. *Adv. Mech. Eng.* **2021**, *13*, 1–22. [CrossRef]
9. Avila, K.; Moxey, D.; De Lozar, A.; Avila, M.; Barkley, D.; Hof, B. The onset of turbulence in pipe flow. *Science* **2011**, *33*, 192–196. [CrossRef]
10. Grossmann, S.; Lohse, D.; Sun, C. High Reynolds numbers Taylor-Couette turbulence. *Annu. Rev. Fluid Mech.* **2016**, *48*, 53–80. [CrossRef]
11. Leclercq, C.; Partridge, J.; Augier, P.; Dalziel, S.; Kerswell, R. Using stratification to mitigate end effects in quasi-Keplerian Taylor-Couette flow. *J. Fluid Mech.* **2016**, *791*, 608–630. [CrossRef]
12. Naimi, M.; Devienne, R.; Lebouche, M. Etude dynamique et thermique de l'écoulement de Couette-Taylor-Poiseuille; cas d'un fluide présentant un seuil d'´écoulement. *Int. J. Heat Mass Transf.* **1990**, *33*, 381. [CrossRef]
13. Jenny, M.; De Richter, S.K.; Louvet, N.; Skali-Lami, S.; Dossmann, Y. Taylor-Couette instability in thixotropic yield stress fluids. *Phys. Rev. Fluids Am. Phys.* **2017**, *2*, 023302. [CrossRef]
14. Huchet, F.; Piton, M.; Del Barrio, A.; Le Corre, O.; Cazacliu, B. Air-cooled heat exchanger applied to external rotary kiln wall in forced and natural draft. *Energy Convers. Manag.* **2017**, *154*, 517–525. [CrossRef]
15. Nouri-Borujerdi, A.; Nakhchi, M.E. Heat transfer enhancement in annular flow with outer grooved cylinder and rotating inner cylinder: Review and experiments. *Appl. Therm. Eng.* **2017**, *120*, 257–268. [CrossRef]
16. Vahl Davis, G.; Thomas, R.W. Natural convection between concentric vertical cylinders. *Phys. Fluids Suppl. II* **1969**, *12*, 198–207.
17. Sorour, M.M.; Coney, J.E.R. The effect of temperature gradient on the stability of flow between vertical, concentric, rotating cylinders. *J. Mech. Eng. Sci.* **1979**, *21*, 403–409. [CrossRef]
18. Lopez, J.M.; Marques, F.; Avila, M. Conductive and convective heat transfer in fluids flows between differentially heated and rotating cylinder. *Int. J. Heat Mass Transf.* **2015**, *90*, 959–967. [CrossRef]
19. Dawood, H.K.; Mohammed, H.A.; Azwadi Che Sidik, N.; Munisamy, K.M.; Wahid, M.A. Forced, natural and mixed-convection heat transfer and fluid flow in annulus: A review. *Int. Commun. Heat Mass Transf.* **2015**, *62*, 45–57. [CrossRef]
20. Avramenko, A.A.; Tyrinov, A.I.; Shevchuk, I.V.; Dmitrenko, N.P. Dean instability of nanofluids with radial temperature and concentration non-uniformity. *Phys. Fluids* **2016**, *28*, 034104. [CrossRef]
21. Davaille, A.; Gueslin, B.; Massmeyer, A.; Giuseppe, E.D. Thermal instabilities in a yield stress fluid: Existence and morphology. *J. Non-Newton. Fluid Mech.* **2013**, *193*, 144–153. [CrossRef]
22. Varé, T.; Nouar, C.; Métivier, C.; Bouteraa, M. Stability of hexagonal pattern in Rayleigh–Bénard convection for thermodependent shear-thinning fluids. *J. Fluid Mech.* **2020**, *905*, A33. [CrossRef]
23. Peixinho, J.; Desaubry, C.; Lebouché, M. Heat transfer of a non-Newtonian fluid (Carbopol aqueous solution) in transitional pipe flow. *Int. J. Heat Mass Transf.* **2008**, *51*, 198–209. [CrossRef]
24. Maleki, A.; Frigaard, I.A. Axial dispersion in weakly turbulent flows of yield stress fluids. *J. Non-Newton. Fluid Mech.* **2016**, *235*, 1–19. [CrossRef]
25. Tso, C.P.; Mahulikar, S.P. Combined evaporating meniscus-driven convection and radiation in annular microchannels for electronics cooling application. *Int. J. Heat Mass Transf.* **2000**, *43*, 1007–1023. [CrossRef]
26. Ozerdem, B. Measurement of convective heat transfer coefficient for a horizontal cylinder rotating in quiescent air. *Int. Commun. Heat Mass Transf.* **2000**, *27*, 389–395. [CrossRef]
27. Harmand, S.; Pellé, J.; Poncet, S.; Shevchuk, I.V. Review of fluid flow and convective heat transfer within rotating disk cavities with impinging jet. *Int. J. Therm. Sci.* **2013**, *67*, 1–30. [CrossRef]
28. Cavazzuti, M.; Agnani, E.; Corticelli, M.A. Optimization of a finned concentric pipes heat exchanger for industrial recuperative burners. *Appl. Therm. Eng.* **2015**, *84*, 110–117. [CrossRef]
29. Douaire, M.; Mercade, M.; Morchain, J.; Loubière, P. A unique phenotypic modification of *Lactococcus lactis* cultivated in a couette bioreactor. *Biotechnol. Bioeng.* **2011**, *108*, 559–571. [CrossRef]
30. Seddegh, S.; Joybari, M.M.; Wang, X.; Haghighat, F. Experimental and numerical characterization of natural convection in a vertical shell-and-tube latent thermal energy storage system. *Sustain. Cities Soc.* **2017**, *35*, 13–24. [CrossRef]
31. Lepiller, V.; Goharzadeh, A.; Prigent, A.; Mutabazi, I. Weak temperature gradient effect on the stability of the circular Couette flow. *Eur. Phys. J. B* **2008**, *61*, 445–455. [CrossRef]
32. Farias, M.H.; Braga, C.V.M.; Souza Mendes, P.R. Heat transfer coefficients for the laminar fully developed flow of viscoplastic liquids through annuli. *Int. J. Heat Mass Transf.* **2009**, *52*, 3257–3260. [CrossRef]
33. Ahmed, H.E.; Ahmed, M.I. Thermal performance of annulus with its applications; A review. *Renew. Sustain. Energy Rev.* **2017**, *71*, 170–190. [CrossRef]

34. Taylor, G.I. Stability of viscous liquid contained between two rotating cylinders. *Philos. Trans. R. Soc. Lond. Ser. A* **1923**, *223*.
35. Coles, D. Transactions in circular Couette flows. *J. Fluid Mech.* **1965**, *21*, 385–425. [CrossRef]
36. Fenstermacher, P.R.; Swinney, H.L.; Gollub, J.P. Dynamical instabilities and the transition to chaotic Taylor vortex flow. *J. Fluid Mech.* **1979**, *94*, 103–128. [CrossRef]
37. Andereck, D.; Liu, S.S.; Swinney, H.L. Flow regimes in a circular Couette system with independently rotating cylinders. *J. Fluid Mech.* **1986**, *164*, 155–183. [CrossRef]
38. Esser, A.; Grossmann, S. Analytic expression for Taylor-Couette stability boundary. *Physic Fluids* **1996**, *8*, 1814. [CrossRef]
39. Domanski, J. Determination of the parameters of fluid motion in Taylor-Couette Flow. *Tech. Sci. Pap. Rep.* **2006**, *9*, 73–78.
40. Kaye, J.; Elgar, E.C. Modes of adiabatic and diabatic fluid flow in an annulus with an inner rotating cylinder. *Trans. ASME* **1958**, *80*, 753–765. [CrossRef]
41. Piton, M. Heat Recovery Exchanger Applied to the Rotary Kiln Equipment. Ph.D. Thesis, Ecole des Mines de Nantes, Nantes, France, 6 November 2015.
42. Chandrasekhar, S. The stability of spiral flow between rotating cylinders. *Proc. R. Soc. Lond. Ser. A* **1962**, *265*, 188–197.
43. Yamada, Y. Resistance of a flow through an annulus with an inner rotating cylinder. *Bull. JSME* **1962**, *5*, 302–310. [CrossRef]
44. Polkowski, J.W. Turbulent flow between coaxial cylinders with the inner cylinder rotating. *J. Eng. Gas Turbines Power* **1984**, *106*, 128–135. [CrossRef]
45. Jakoby, R.; Kim, S.; Wittig, S. Correlations of the convection heat transfer in annular channels with rotating inner cylinder. *J. Eng. Gas Turbines Power* **1999**, *121*, 670–677. [CrossRef]
46. Lueptow, R.M.; Docter, A.; Min, K. Stability of axial flow in an annulus with a rotating inner cylinder. *Phys. Fluids* **1992**, *A4*, 2446–2456. [CrossRef]
47. Wan, C.C.; Coney, J.E.R. Transition modes in adiabatic spiral vortex flow in narrow and wide annular gaps. *Int. J. Heat Fluid Flow* **1980**, *2*, 131–138. [CrossRef]
48. Molki, M.; Astill, K.N.; Leal, E. Convective heat-mass transfer in the entrance region of a concentric annulus having a rotating inner cylinder. *Int. J. Heat Fluid Flow* **1990**, *11*, 120–128. [CrossRef]
49. Fénot, M.; Bertin, Y.; Dorignac, E.; Lalizel, G. A review of heat transfer between concentric rotating cylinders with or without axial flow. *Int. J. Therm. Sci.* **2011**, *50*, 1138–1155. [CrossRef]
50. Nourri, J.M.; Whitelaw, J.H. Flow of Newtonian and non-Newtonian fluids in a concentric annulus with rotation of inner cylinder. *J. Fluid Eng.* **1994**, *116*, 821–827. [CrossRef]
51. Escudier, M.P.; Gouldson, I.W. Concentric annular flow with centerbody rotation of a Newtonian and a shear-thinnig liquid. *Int. J. Heat Fluid Flow* **1995**, *16*, 156–162. [CrossRef]
52. Chung, S.Y.; Rhee, G.H.; Sung, H.J. Direct numerical simulation of turbulent concentric annular pipe flow. Part. 1: Flow field. *Int. J. Heat Fluid Flow* **2002**, *23*, 426–440. [CrossRef]
53. Chung, S.Y.; Sung, H.J. Large-eddy simulation of turbulent flow in concentric annulus with rotation of an inner cylinder. *Int. J. Heat Fluid Flow* **2005**, *26*, 191–203. [CrossRef]
54. Jung, S.Y.; et Sung, H.J. Characterization of the three-dimensional turbulent boundary layer in a concentric annulus with a rotating inner cylinder. *Phys. Fluids* **2006**, *18*, 115102. [CrossRef]
55. Hadziabdic, M.; Hanjalic, K.; Mullyadzhanov, R. LES of turbulent flow in a concentric annulus with rotating outer wall. *Int. J. Heat Fluid Flow* **2013**, *43*, 74–84. [CrossRef]
56. Poncet, S.; Viazzo, S.; Oguic, R. Large eddy simulation of Taylor-Couette-Poiseuille flows in a narrow-gap system. *Phys. Fluids* **2014**, *26*, 105108. [CrossRef]
57. Poncet, S.; Haddadi, S.; Viazzo, S. Numerical modeling of fluid flow and heat transfer in a narrow Taylor-Couette-Poiseuille system. *Int. J. Heat Fluid Flow* **2011**, *32*, 128–144. [CrossRef]
58. Pawar, S.B.; Thorat, B.N. CFD simulation of Taylor-Couette flow in scraped surface heat exchanger. *Chem. Eng. Res. Des.* **2012**, *90*, 313–322. [CrossRef]
59. Naser, A. Prediction of Newtonian and non-Newtonian flow through concentric annulus with centerbody rotation. In Proceedings of the 1st International Conference on CFD in Mineral and Metal Processing and Power Generation, Melbourne, Australia, 3–4 July 1997.
60. Ohsawa, A.; Murata, A.; Iwamoto, K. Through-flow effects on Nusselt number and torque coefficient in Taylor-Couette-Poiseuille flow investigated by large eddy simulation. *J. Therm. Sci. Technol.* **2016**, *11*, 1–12. [CrossRef]
61. Mehrez, I.; Gheith, R.; Aloui, F.; Nasrallah, S.B. Theoretical and numerical study of Couette-Taylor flow with an axial flow-using lattice Boltzmann method. *Int. J. Numer. Meth. Fluids* **2019**, *90*, 427–441. [CrossRef]
62. Piton, M.; Huchet, F.; Cazacliu, B.; Le Corre, O. Numerical Turbulent Flow Analysis through a Rotational Heat Recovery System. *Energies* **2022**, *15*, 6792. [CrossRef]
63. Guillerm, R.; Kang, C.; Savaro, C.; Lepiller, V.; Prigent, A.; Yang, K. Flow regimes in a vertical Taylor-Couette system with a radial thermal gradient. *Phys. Fluids* **2015**, *27*, 094101. [CrossRef]
64. Bjorklund, I.; Kays, W. Heat transfer between concentric rotating cylinders. *Trans. ASME J. Heat Transf.* **1959**, *84*, 97–105. [CrossRef]
65. Vafai, K.; Desai, C.P.; Iyer, S.V.; Dyko, M.P. Buoyancy induced convection in a narrow open-ended annulus. *J. Heat Transf.* **1997**, *19*, 483–494. [CrossRef]
66. Grossman, S.; Lohse, D. Multiple scaling in the ultimate regime of thermal convection. *Phys. Fluids* **2011**, *23*, 045108. [CrossRef]

67. Boffeta, G.; Mazzino, A. Incompressible Rayleigh-Taylor turbulence. *Annu. Rev. Fluid Mech.* **2017**, *49*, 119–143. [CrossRef]
68. Leng, X.Y.; Zhong, J.Q. Mutual coherent structures for heat and angular momentum transport in turbulent Taylor-Couette flows. *Phys. Rev. Fluids* **2022**, *7*, 043501. [CrossRef]
69. Howey, D.A.; Childs, P.R.N.; Holmes, A.S. Air-Gap convection in rotating electrical machines. *IEEE Trans. Ind. Electron.* **2012**, *59*, 1367–1375. [CrossRef]
70. Nouri-Borujerdi, A.; Nakhchi, M.E. Optimization of the heat transfer coefficient and pressure drop of Taylor-Couette-Poiseuille flows between an inner rotating cylinder and an outer grooved stationary cylinder. *Int. J. Heat Mass Transf.* **2017**, *108*, 1449–1459. [CrossRef]
71. Becker, K.; Kaye, J. The influence of a radial temperature gradient on the instability of fluid flow in an annulus with inner rotating cylinder. *Trans. ASME* **1962**, *80*, 79–90. [CrossRef]
72. Gazley, C. Heat-Transfer Characteristics of the Rotational and Axial Flow between Concentric Cylinders. *J. Turbomach.* **1958**, *80*, 79–90. [CrossRef]